

Topological Insulator and Helical Zero Mode in Silicene under Inhomogeneous Electric Field

Motohiko Ezawa

Department of Applied Physics, University of Tokyo, Hongo 7-3-1, 113-8656, Japan

Silicene is a monolayer of silicon atoms forming a two-dimensional honeycomb lattice, which shares almost every remarkable property with graphene. The low energy structure of silicene is described by Dirac electrons with relatively large spin-orbit interactions due to its buckled structure. The key observation is that the band structure is controllable by applying the electric field to a silicene sheet. In particular, the gap closes at a certain critical electric field. Examining the band structure of a silicene nanoribbon, we demonstrate that a topological phase transition occurs from a topological insulator to a band insulator with the increase of the electric field. We also show that it is possible to generate helical zero modes anywhere in a silicene sheet by adjusting the electric field locally to this critical value. The region may act as a quantum wire or a quantum dot surrounded by topological and/or band insulators. We explicitly construct the wave functions for some simple geometries based on the low-energy effective Dirac theory. These results are applicable also to germanene, that is a two-dimensional honeycomb structure of germanium.

I. INTRODUCTION

Graphene, a monolayer honeycomb structure of carbon atoms, is one of the most important topics in condensed matter physics¹. One of the obstacles of graphene for electronic devices is that electrons can not be confined by applying external electric field². Thus, graphene nanostructures such as graphene nanoribbon³ and nanodisk⁴ have been considered, which are to be fabricated by cutting a graphene sheet. Recently a new material, a monolayer honeycomb structure of silicon called silicene, has been synthesized⁵⁻⁷ and attracts much attention⁸⁻¹⁰. Silicene has Dirac cones akin to graphene. Almost every striking property of graphene could be transferred to this innovative material. Furthermore, silicene has advantage of easily being incorporated into the silicon-based electronic technology.

Silicene has a remarkable property graphene does not share: It is the buckled structure^{9,10} owing to a large ionic radius of silicon (Fig.1). Consequently, silicene has a relatively large spin-orbit (SO) gap of 1.55meV, as makes experimentally accessible the Kane-Mele type quantum Spin Hall (QSH) effect or topological insulator^{9,10}. Topological insulator^{11,12} is a new state of quantum matter characterized by a full insulating gap in the bulk and gapless edges topologically protected. These states are made possible due to the combination of the SO interaction and the time-reversal symmetry. The two-dimensional topological insulator is a QSH insulator with helical gapless edge modes¹³, which is a close cousin of the integer quantum Hall state. QSH insulator was proposed by Kane and Mele in graphene¹⁴. However, since the SO gap is rather weak in graphene, the QSH effect can occur in graphene only at unrealistically low temperature^{15,16}.

The buckled structure implies an intriguing possibility that we can control the band structure by applying the electric field (Fig.1). In this paper, we analyze the band structure under the electric field E_z applied perpendicular to a silicene sheet. Silicene is a \mathbb{Z}_2 topological insulator⁹ at $E_z = 0$. By increasing E_z , we demonstrate the following. The gap decreases linearly to zero at a certain critical field E_c and then increases linearly. Accordingly, silicene undergoes a topological phase transition

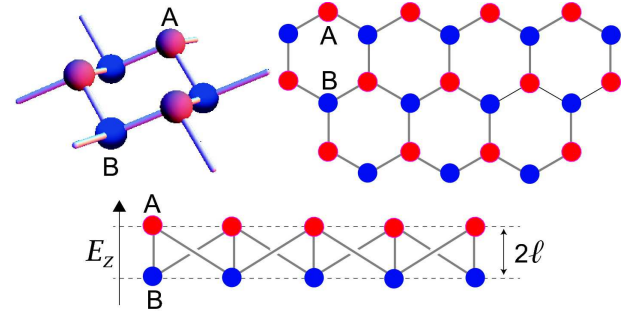


FIG. 1: (Color online) Illustration of the buckled honeycomb lattice of silicene. A honeycomb lattice is distorted due to a large ionic radius of a silicon atom and forms a buckled structure. The A and B sites form two sublattices separated by a perpendicular distance 2ℓ . The structure generates a staggered sublattice potential in the electric field E_z , which leads to various intriguing phenomena.

from a topological insulator to a band insulator. At the critical point ($E_z = E_c$), spins are perfectly spin-up (spin-down) polarized at the K (K') point.

We also investigate the zero-energy states under an inhomogeneous electric field $E_z(x, y)$ based on the low-energy effective Dirac theory. There emerge helical zero modes in the region where $E_z(x, y) = E_c$. It is intriguing that the region is not necessary one-dimensional: The region can be two-dimensional and have any shape, where Dirac electrons can be confined. It is surrounded by topological and/or band insulators. Our result may be the first example in which helical zero modes appear in regions besides the edge of a topological insulator. The region may act as a quantum wire or a quantum dot. We construct explicitly the wave functions describing helical zero modes for regions having simple geometries. In conclusion, we are able to realize a dissipationless spin current anywhere in the bulk of a silicene sheet by tuning the electric field locally.

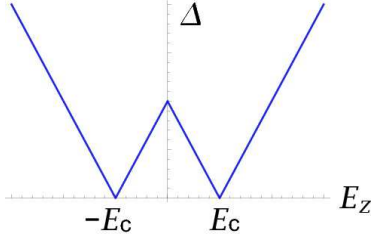


FIG. 2: (Color online) The band gap Δ as a function of the electric field E_z . The gap is open for $E_z \neq \pm E_c$, where silicene is an insulator. It can be shown that it is a topological insulator for $|E_z| < E_c$ and a band insulator $|E_z| > E_c$.

II. TOPOLOGICAL AND BAND INSULATORS

Silicene consists of a honeycomb lattice of silicon atoms with two sublattices made of A sites and B sites. The states near the Fermi energy are π orbitals residing near the K and K' points at opposite corners of the hexagonal Brillouin zone. We take a silicene sheet on the xy -plane, and apply the electric field $E_z(x, y)$ perpendicular to the plane. Due to the buckled structure the two sublattice planes are separated by a distance, which we denote by 2ℓ with $\ell = 0.23\text{\AA}$, as illustrated in Fig.1. It generates a staggered sublattice potential $\propto 2\ell E_z(x, y)$ between silicon atoms at A sites and B sites.

The silicene system is described by the four-band second-nearest-neighbor tight binding model¹⁰,

$$\begin{aligned}
 H = & -t \sum_{\langle i,j \rangle \alpha} c_{i\alpha}^\dagger c_{j\alpha} + i \frac{\lambda_{\text{SO}}}{3\sqrt{3}} \sum_{\langle\langle i,j \rangle\rangle \alpha\beta} \nu_{ij} c_{i\alpha}^\dagger \sigma_{\alpha\beta}^z c_{j\beta} \\
 & - i \frac{2}{3} \lambda_{\text{R}} \sum_{\langle\langle i,j \rangle\rangle \alpha\beta} \mu_{ij} c_{i\alpha}^\dagger \left(\vec{\sigma} \times \vec{d}_{ij}^0 \right)_{\alpha\beta}^z c_{j\beta} \\
 & + \ell \sum_{i\alpha} \zeta_i E_z c_{i\alpha}^\dagger c_{i\alpha}.
 \end{aligned} \quad (2.1)$$

The first term represents the usual nearest-neighbor hopping on the honeycomb lattice with the transfer energy $t = 1.6\text{eV}$, where the sum is taken over all pairs $\langle i, j \rangle$ of the nearest-neighboring sites, and the operator $c_{i\alpha}^\dagger$ creates an electron with spin polarization α at site i . The second term represents the effective SO coupling with $\lambda_{\text{SO}} = 3.9\text{meV}$, where $\vec{\sigma} = (\sigma^x, \sigma^y, \sigma^z)$ is the Pauli matrix of spin, $\nu_{ij} = (\vec{d}_i \times \vec{d}_j) / |\vec{d}_i \times \vec{d}_j|$ with \vec{d}_i and \vec{d}_j the two nearest bonds connecting the next-nearest neighbors, and the sum is taken over all pairs $\langle\langle i, j \rangle\rangle$ of the second-nearest-neighboring sites. The third term represents the Rashba SO coupling with $\lambda_{\text{R}} = 0.7\text{meV}$, where $\mu_{ij} = \pm 1$ for the A (B) site, and $\vec{d}_{ij}^0 = \vec{d}_{ij} / |\vec{d}_{ij}|$. The forth term is the staggered sublattice potential term, where $\zeta_i = \pm 1$ for the A (B) site. Note that the first and the second terms constitute the Kane-Mele model proposed to demonstrate the QSH effect in graphene¹⁴.

The same Hamiltonian as (2.1) can be used to describe germanene, that is a honeycomb structure of germanium^{9,10},

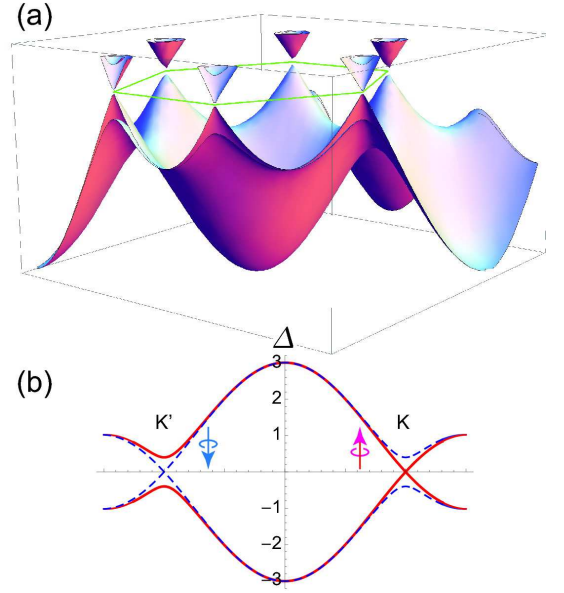


FIG. 3: (Color online) Band structure of silicene at the critical electric field E_c . (a) A bird's-eye view. Dirac cones are found at 6 corners of the hexagonal Brillouin zone. (b) The cross section containing a pair of K and K' points. The solid red (dashed blue) band is for up-spin (down-spin) electrons, which are gapless (gapped) at the K point but gapped (gapless) at the K' point.

where various parameters are $t = 1.3\text{eV}$, $\lambda_{\text{SO}} = 43\text{meV}$, $\lambda_{\text{R}} = 10.7\text{meV}$ and $\ell = 0.33\text{\AA}$. Hence the following analysis is applicable to germanene as well.

We study the band structure of silicene by applying a uniform electric field E_z . By diagonalizing the Hamiltonian (2.1), the band gap $\Delta(E_z)$ is determined to be

$$\Delta(E_z) = 2|\ell E_z - \eta s_z \lambda_{\text{SO}}|, \quad (2.2)$$

where $s_z = \pm 1$ is the electron spin and $\eta = \pm 1$ is for the K or K' point (to which we refer also as the K_\pm point). See also the dispersion relation (3.4) which we derive based on the low-energy effective theory. We emphasize that it is independent of the Rashba SO coupling λ_{R} . The gap (2.2) vanishes at $E_z = \eta s_z E_c$ with

$$E_c = \lambda_{\text{SO}}/\ell = 17\text{meV/\AA}. \quad (2.3)$$

We plot the band gap $\Delta(E_z)$ in the Fig.2.

The gap closes at $E_z = \pm E_c$, where it is a semimetal due to gapless modes. We show the band structure at $E_z = E_c$ in Fig.3. It follows from (2.2) that up-spin ($s_z = +1$) electrons are gapless at the K point ($\eta = +1$), while down-spin ($s_z = -1$) electrons are gapless at the K' point ($\eta = -1$). Namely, spins are perfectly up (down) polarized at the K (K') point under the uniform electric field $E_z = E_c$.

It follows from the gap formula (2.2) that silicene is an insulator for $E_z \neq \pm E_c$. In order to tell the difference between the two insulators realized for $|E_z| < E_c$ and $|E_z| > E_c$, we study the band structure of a silicene nanoribbon with zigzag edges. The gap structure is depicted at two typical points,

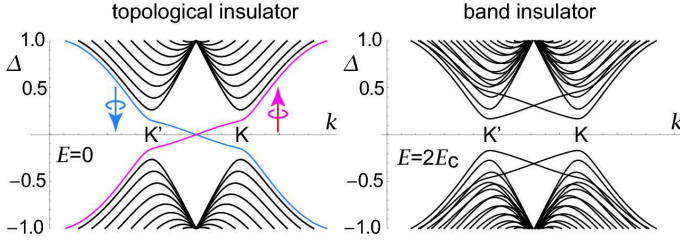


FIG. 4: (Color online) One-dimensional energy bands for a silicene nanoribbon. (a) The bands crossing the gap are edge states, demonstrating that it is a topological insulator. There are two edge states since a nanoribbon has two edges (red and blue lines for the left and right edges). (b) All states are gapped, demonstrating that it is a band insulator.

$E_z = 0$ and $E_z = 2E_c$, in Fig.4. We see that there are gapless modes coming from the two edges at $|E_z| < E_c$, as is the demonstration of a topological insulator⁹. On the other hand, there are no gapless edge modes for $|E_z| > E_c$, showing that it is a band insulator. We conclude that a topological phase transition occurs between a topological insulator ($|E_z| < E_c$) and a band insulator ($|E_z| > E_c$) as E_z changes.

The reason why gapless modes appear in the edge of a topological insulator is understood as follows. The topological insulator has a nontrivial topological number, the \mathbb{Z}_2 index¹⁴, which is defined only for a gapped state. When a topological insulator has an edge beyond which the region has the trivial \mathbb{Z}_2 index, the band must close and yield gapless modes in the interface. Otherwise the \mathbb{Z}_2 index cannot change its value across the interface.

III. LOW-ENERGY DIRAC THEORY

We proceed to analyze the physics of electrons near the Fermi energy more in details. The low-energy Dirac theory has been proved to be essential in the study of graphene¹⁷ and its various derivatives^{18,19}. It must also be indispensable to explore deeper physics of helical zero modes and promote further researches in silicene.

We may derive the low-energy effective Hamiltonian from the tight binding model (2.1) around the K_η point as¹⁰

$$H_\eta = \hbar v_F (k_x \tau_x - \eta k_y \tau_y) + \eta \tau_z h_{11} + \ell E_z \tau_z, \quad (3.1)$$

with

$$h_{11} = -\lambda_{SO} \sigma_z - a \lambda_R (k_y \sigma_x - k_x \sigma_y), \quad (3.2)$$

where τ_a is the Pauli matrix of the sublattice, $v_F = \frac{\sqrt{3}}{2} a t = 5.5 \times 10^5 \text{ m/s}$ is the Fermi velocity, and $a = 3.86 \text{ \AA}$ is the lattice constant. It is instructive to write down the Hamiltonian H_+ explicitly as

$$\begin{pmatrix} -\lambda_{SO} + \ell E_z & v_F k_+ & i a \lambda_R k_- & 0 \\ v_F k_- & \lambda_{SO} - \ell E_z & 0 & -i a \lambda_R k_- \\ -i a \lambda_R k_+ & 0 & \lambda_{SO} + \ell E_z & v_F k_+ \\ 0 & i a \lambda_R k_+ & v_F k_- & -\lambda_{SO} - \ell E_z \end{pmatrix} \quad (3.3)$$

in the basis $\{\psi_{A\uparrow}, \psi_{B\uparrow}, \psi_{A\downarrow}, \psi_{B\downarrow}\}^t$, where $k_\pm = k_x \pm i k_y$. The two Hamiltonians H_+ and H_- are related through the time-reversal operation.

The energy spectrum is readily derived from (3.1),

$$\mathcal{E}_\eta = \pm \sqrt{\hbar^2 v_F^2 k^2 + \left(\ell E_z - \eta s_z \sqrt{\lambda_{SO}^2 + a^2 \lambda_R^2} k^2 \right)^2}, \quad (3.4)$$

which yields the result (2.2) to the gap energy at $k = 0$.

IV. INHOMOGENEOUS ELECTRIC FIELD

The low-energy Dirac theory allows us to investigate analytically the properties of the helical zero mode under inhomogeneous electric field. In so doing we set $\lambda_R = 0$ to simplify calculations. This approximation is justified by the following reasons. First all, we have numerically checked that the band structure is rather insensitive to λ_R based on the tight-binding Hamiltonian (2.1). Second, λ_R appears only in the combination $\lambda_R k_\pm$ in the Hamiltonian (3.1), which vanishes exactly at the K_\pm points. Third, the critical electric field E_c is independent of λ_R as in (2.3).

A. Inhomogeneous electric field along x -axis

We apply the electric field $E_z(x)$ perpendicularly to a silicene sheet homogeneously in the y direction and inhomogeneously in the x direction. We may set $k_y = \text{constant}$ due to the translational invariance along the y axis. The momentum k_y is a good quantum number. Setting

$$\Psi(x, y) = e^{i k_y y} \Phi(x), \quad (4.1)$$

we seek the zero-energy solution, where $\Psi(x, y)$ is a four-component amplitude. The particle-hole symmetry guarantees the existence of zero-energy solutions satisfying the relation $\phi_B(x) = i \xi \phi_A(x)$ with $\xi = \pm 1$. Here, ϕ_A is a two-component amplitude with the up spin and the down spin. Then the eigenvalue problem yields

$$H_\eta \phi_A(x) = E_\eta \phi_A(x), \quad (4.2)$$

together with a linear dispersion relation

$$E_\eta \xi = \eta \xi \hbar v_F k_y. \quad (4.3)$$

The equation of motion for $\phi_A(x)$ reads

$$(\xi \hbar v_F \partial_x + \eta \lambda_{SO} \sigma_z - \ell E_z(x)) \phi_A(x) = 0. \quad (4.4)$$

We can explicitly solve this as

$$\phi_{As_z}(x) = C \exp f(x), \quad (4.5)$$

with

$$f(x) = C \exp \left[\frac{\xi}{\hbar v_F} \int^x (-\eta s_z \lambda_{SO} + \ell E_z(x')) dx' \right], \quad (4.6)$$

where C is the normalization constant. The sign ξ is determined so as to make the wave function finite in the limit $|x| \rightarrow \infty$. The current is calculated as

$$J_{s_z}(x) = \text{Re} \left[\frac{\hbar}{2mi} \Psi_{s_z}^\dagger \partial_y \Psi_{s_z} \right] = \frac{\hbar k_y}{m} |\phi_{As_z}(x)|^2. \quad (4.7)$$

This is a reminiscence of the Jackiw-Rebbi mode²⁰ proposed for the chiral mode.

The difference between the chiral and helical modes is the presence of the spin factor s_z in the wave function. As we shall see explicitly in some examples in what follows, we find the condition either $\eta s_z = 1$ or $\eta s_z = -1$ for convergence of the wave function. The condition $\eta s_z = 1$ implies that the spin is up ($s_z = 1$) at the K point ($\eta = 1$) and that the spin is down ($s_z = -1$) at the K' point ($\eta = -1$). Consequently, the up-spin electrons flow into the positive x -direction while the down-spin electrons flow into the negative x -direction, implying that the pure spin current flows into the positive x -direction. On the other hand, the condition $\eta s_z = -1$ implies that the pure spin current flows into the negative x -direction.

Interface between topological and band insulators: We apply an electric field such that

$$E_z(x) = \alpha x / \ell. \quad (4.8)$$

Substituting it to (4.6), we obtain

$$f(x) = \frac{\xi \alpha}{2\hbar v_F} \left\{ \left(x - \frac{\eta s_z \lambda_{SO}}{\alpha} \right)^2 - \left(\frac{\eta s_z \lambda_{SO}}{\alpha} \right)^2 \right\}, \quad (4.9)$$

where ξ is chosen to make $\xi \alpha < 0$ for convergence. The wave function is localized along the two lines $x = \eta s_z \lambda_{SO} / \alpha = \pm \lambda_{SO} / \alpha$ taken in the bulk, where the gapless mode emerges since $E_z(x) = \pm \lambda_{SO}$. The currents are helical along these two lines, where $\eta s_z = 1$ along one line and $\eta s_z = -1$ along the other line: The spin currents flow in the opposite directions along these two lines, sandwiched by a band insulator ($|x| > \lambda_{SO} / |\alpha|$) and a topological insulator ($|x| < \lambda_{SO} / |\alpha|$). We illustrate the probability density $|\phi_{As_z}(x)|^2$ in Fig.5(a) in the case $\alpha > 0$. Each line may be used as a quantum wire.

Interface between metal and insulator: We apply an electric field such that

$$E_z(x) = E_c + \frac{\alpha x}{\ell} \Theta(x), \quad (4.10)$$

where $\Theta(x)$ is the step function: $\Theta(x) = 0$ for $x < 0$ and $\Theta(x) = 1$ for $x \geq 0$. Substituting it to (4.6), we obtain

$$f(x) = \frac{\xi}{\hbar v_F} \left\{ \frac{\alpha x^2}{2} \Theta(x) + (1 - \eta s_z) \lambda_{SO} x \right\}, \quad (4.11)$$

where ξ is chosen to make $\xi \alpha < 0$ for convergence. Namely, when we choose $\alpha > 0$, we find

$$\begin{aligned} E_z(x) &= E_c \quad (\text{metal}) \quad \text{for } x \leq 0 \\ E_z(x) &> E_c \quad (\text{BI}) \quad \text{for } x > 0, \end{aligned} \quad (4.12)$$

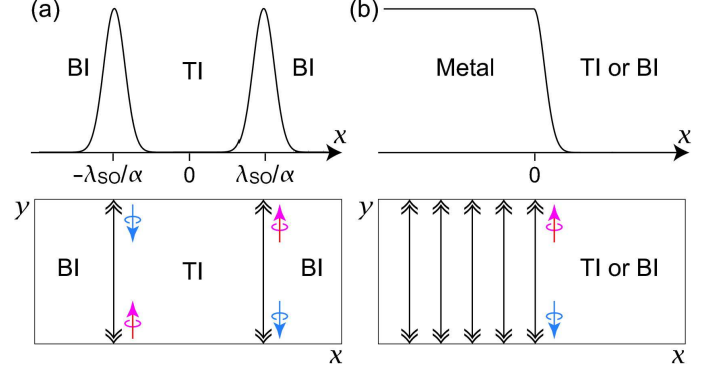


FIG. 5: (Color online) The probability density of the helical zero mode under the electric field E_z . (a) E_z is given by (4.8) with $\alpha > 0$. The spin current flows between a topological insulator and a band insulator. (b) E_z is given by (4.10) with $\alpha > 0$. The spin current flows in the metallic region. The arrows indicate the helical mode with spin up at the K point and with spin down at the K' point.

and when we choose $\alpha < 0$, we find

$$\begin{aligned} E_z(x) &= E_c \quad (\text{metal}) \quad \text{for } x \leq 0 \\ E_z(x) &< E_c \quad (\text{TI}) \quad \text{for } x > 0, \end{aligned} \quad (4.13)$$

where TI and BI stand for topological and band insulators. In the both cases the region $x \leq 0$ is a metal. Furthermore, it is necessary that $\eta s_z = 1$ for convergence of the wave function, as implies that the current is helical in the metallic region. We illustrate the probability density $|\phi_{A\uparrow}(x)|^2$ in Fig.5(b) in the case $\alpha > 0$, which is a constant for $x \leq 0$.

It is intriguing that there emerge helical zero modes in metal. This is not surprising because the edge of a topological insulator is a sufficient condition but not a necessary condition for the emergence of helical zero modes. The helical zero mode requires the massless Dirac fermion, the time-reversal symmetry and the spin-orbit interaction. Our example shows explicitly that it can appear in regions besides the edge of a topological insulator provided these conditions are satisfied.

B. Inhomogeneous electric field along r -axis

We apply a cylindrical symmetric inhomogeneous electric field $E_z(r)$ to a silicene sheet. The equation reads

$$\begin{pmatrix} -\lambda_{SO}\sigma_z + \ell E_z(r) & \hbar v_F e^{i\theta} (i\partial_r - \frac{1}{r}\partial_\theta) \\ \hbar v_F e^{-i\theta} (i\partial_r + \frac{1}{r}\partial_\theta) & \lambda_{SO}\sigma_z - \ell E_z(r) \end{pmatrix} \begin{pmatrix} \psi_A \\ \psi_B \end{pmatrix} = 0. \quad (4.14)$$

We solve this for zero-energy states by setting

$$\begin{pmatrix} \psi_A(r, \theta) \\ \psi_B(r, \theta) \end{pmatrix} = \begin{pmatrix} e^{i\eta\theta/2} \phi_A(r) \\ e^{-i\eta\theta/2} \phi_B(r) \end{pmatrix}. \quad (4.15)$$

The equation of motion $H_K \psi = 0$ is transformed into

$$\left(\xi \hbar v_F \left(\partial_r + \frac{1}{2r} \right) + \eta \lambda_{SO} \sigma_z - \ell E_z(r) \right) \phi_A = 0, \quad (4.16)$$

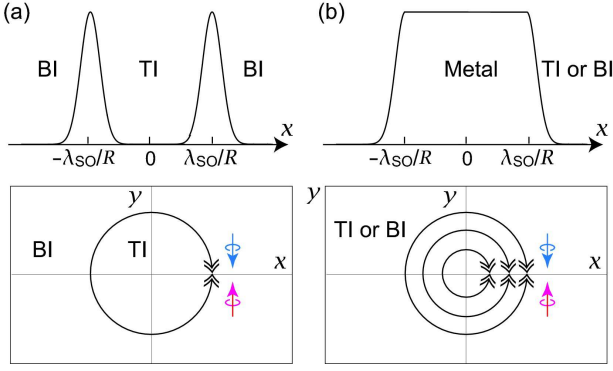


FIG. 6: (Color online) The probability density of the helical zero mode under the electric field E_z with $\alpha > 0$. (a) E_z is given by (4.19). The spin current flows between a topological insulator and a band insulator by encircling the topological insulator. (b) E_z is given by (4.21) with $\alpha > 0$. The spin current flows in the disklike metallic region confined within a topological or band insulator. The arrows indicate the helical mode with spin up at the K point and with spin down at the K' point.

which we solve as

$$\phi_{As_z}(r) = \frac{C}{\sqrt{r}} \exp f(r), \quad (4.17)$$

with

$$f(r) = \frac{\xi}{\hbar v_F} \int_0^r (-\eta s_z \lambda_{SO} + \ell E_z(r')) dr', \quad (4.18)$$

where C is the normalization constant and $\xi = \pm 1$. The sign ξ is determined so as to make the wave function finite in the limit $r \rightarrow \infty$.

Interface between topological and band insulators: We apply an electric field such that

$$E_z(r) = \alpha r / \ell. \quad (4.19)$$

Substituting it to (4.18), we have

$$f(r) = \frac{\xi \alpha}{2 \hbar v_F} \left\{ \left(r - \frac{\eta s_z \lambda_{SO}}{\alpha} \right)^2 - \left(\frac{\eta s_z \lambda_{SO}}{\alpha} \right)^2 \right\}. \quad (4.20)$$

where ξ is chosen to make $\xi \alpha < 0$ for convergence. The wave function is localized along the circle $r = \eta s_z \lambda_{SO} / \alpha > 0$, where $E_z(r) = \pm \lambda_{SO}$. When we choose $\alpha > 0$ it is necessary that $\eta s_z = 1$, and when we choose $\alpha < 0$ it is necessary that $\eta s_z = -1$. In any of the two cases, there emerges helical zero modes and the spin current flows along the circle between a topological insulator ($r < \lambda_{SO}/|\alpha|$) and a band insulator ($r > \lambda_{SO}/|\alpha|$). The direction of the spin current is opposite for $\alpha > 0$ and $\alpha < 0$. We illustrate the probability density

$|\phi_{As_z}(r)|^2$ in Fig.6(a) in the case $\alpha > 0$. This region may be used as a quantum wire.

Interface between metal and insulator: We apply an electric field such that

$$E_z(r) = E_c + \frac{\alpha(r-R)}{\ell} \Theta(r-R), \quad (4.21)$$

where $\Theta(r)$ is the step function. Substituting it to (4.18), we have

$$f(r) = \frac{\xi}{\hbar v_F} \left\{ \frac{\alpha(r-R)^2}{2\ell} \Theta(r-R) + (1 - \eta s_z) \lambda_{SO}(r-R) \right\}, \quad (4.22)$$

where ξ is chosen to make $\xi \alpha < 0$ for convergence. It is notable that $E_z(r) = E_c$ for $r < R$ and hence the system is metallic there. The wave function describes an interface between a metal for $r < R$ and an insulator for $r > R$. The insulator is a topological insulator when we choose $\alpha < 0$ and a band insulator when we choose $\alpha > 0$. Since it is necessary that $\eta s_z = 1$ for convergence of the wave function, the current is helical in the metallic region ($r \leq R$). We show the probability density $|\phi_{A\uparrow}(r)|^2$ in Fig.6(b), where $\phi_{A\uparrow}(r) = \text{constant}$ for $r \leq R$. This region may act as a quantum dot.

V. CONCLUSIONS

Taking advantage of the buckled structure of silicene we have demonstrated that we can control its band structure by applying the electric field E_z . Silicene undergoes a topological phase transition between a topological insulator and a band insulator as E_z crosses the critical point $\pm E_c$. It is a semimetal at $E_z = \pm E_c$.

A novel phenomenon appears when we apply an inhomogeneous electric field. We have explicitly constructed wave functions of helical zero modes for simple geometrical regions based on the low-energy effective Dirac theory. The results imply in general that helical zero modes can be confined in any regions by tuning the external electric field locally to the critical field (2.3), $E_z(x, y) = E_c$. Our system may be the first example in which helical zero modes appear in regions besides the edge of a topological insulator. It is to be emphasized that we can apply an inhomogeneous electric field so that a single silicene sheet contains several regions which are topological insulators, band insulators and metals. Such a structure may open a way for future spintronics. Our results are also applicable to germanene, that is a two-dimensional honeycomb structure made of germanium.

I am very much grateful to N. Nagaosa for many fruitful discussions on the subject. This work was supported in part by Grants-in-Aid for Scientific Research from the Ministry of Education, Science, Sports and Culture No. 22740196.

¹ A.H. Castro Neto, F. Guinea, N.M.R. Peres, K.S. Novoselov and A.K. Geim, Rev. Mod. Phys. **81**, 109 (2009).

² M.I. Katsnelson, K.S. Novoselov and A.K. Geim, Nature Physics

- 2, 620 (2006).
- ³ M. Fujita, K. Wakabayashi, K. Nakada, and K. Kusakabe, J. Phys. Soc. Jpn. **65**, 1920 (1996); M. Ezawa, Phys. Rev. B **73**, 045432 (2006).
- ⁴ M. Ezawa, Phys. Rev. B **76**, 245415 (2007); J. Fernández-Rossier and J. J. Palacios, Phys. Rev. Lett. **99**, 177204 (2007).
- ⁵ B. Lalmi, H. Oughaddou, H. Enriquez, A. Kara, S. Vizzini, B. Ealet, and B. Aufray, Appl. Phys. Lett. **97**, 223109 (2010).
- ⁶ P.E. Padova, C. Quaresima, C. Ottaviani, P.M. Sheverdyaeva, P. Moras, C. Carbone, D. Topwal, B. Olivieri, A. Kara, H. Oughaddou, B. Aufray, and G.L. Lay, Appl. Phys. Lett. **96**, 261905 (2010).
- ⁷ B. Aufray A. Vizzini, H. Oughaddou, C. Lndri, B. Ealet, and G.L. Lay, Appl. Phys. Lett. **96**, 183102 (2010).
- ⁸ Gian G. Guzmán-Verri and L. C. Lew Yan Voon, Phys. Rev. B **76** (2007) 075131.
- ⁹ C.-C. Liu, W. Feng, and Y. Yao, Phys. Rev. Lett. **107**, 076802 (2011).
- ¹⁰ C.-C. Liu, H. Jiang, and Y. Yao, Phys. Rev. B, **84**, 195430 (2011).
- ¹¹ M.Z Hasan and C. Kane, Rev. Mod. Phys. **82**, 3045 (2010).
- ¹² X.-L. Qi and S.-C. Zhang, Rev. Mod. Phys. **83**, 1057 (2011).
- ¹³ C. Wu, B.A. Bernevig and S.-C. Zhang, Phys. Rev. Lett. **96**, 106401 (2006).
- ¹⁴ C. L. Kane and E. J. Mele, Phys. Rev. Lett. **95**, 226801 (2005); *ibid* **95**, 146802 (2005).
- ¹⁵ H. Min, J.E. Hill, N.A. Sinitsyn, B.R. Sahu, L. Kleinman, and A.H. MacDonald, Phys. Rev. B **74**, 165310 (2006).
- ¹⁶ Y. Yao, F. Ye, X.-L. Qi, S.-C. Zhang, and Z. Fang, Phys. Rev. B **75**, 041401 (2007).
- ¹⁷ J.C. Slonczewski and P.R. Weiss: Phys. Rev. **109**, (1958) 272; G.W. Semenoff, Phys. Rev. Lett. **53**, 2449 (1984).
- ¹⁸ L. Brey and H.A. Fertig, Phys. Rev. B **73**, 235411 (2006).
- ¹⁹ M. Ezawa, Phys. Rev. B **81**, 201402R (2010).
- ²⁰ R. Jackiw and C. Rebbi, Phys. Rev. D **13**, 3398 (1976).